

Dissimilar thermal transport properties in κ -Ga₂O₃ and β -Ga₂O₃ revealed by machine-learning homogeneous nonequilibrium molecular dynamics simulations

Xiaonan Wang,¹ Jinfeng Yang,¹ Penghua Ying,^{1, a)} Zheyong Fan,² Jin Zhang,¹ and Huarui Sun^{1, 3, b)}

¹⁾*School of Science, Harbin Institute of Technology, Shenzhen, 518055,*

P. R. China

²⁾*College of Physical Science and Technology, Bohai University, Jinzhou 121013,*

P. R. China

³⁾*Ministry of Industry and Information Technology Key Laboratory of Micro-Nano Optoelectronic Information System, Harbin Institute of Technology, Shenzhen, 518055, P. R. China.*

(Dated: 3 November 2023)

The lattice thermal conductivity (LTC) of Ga₂O₃ is an important property due to the challenge in the thermal management of high-power devices. We develop machine-learned neuroevolution potentials for single-crystalline β -Ga₂O₃ and κ -Ga₂O₃, and apply them to perform homogeneous nonequilibrium molecular dynamics simulations to predict their LTCs. The LTC of β -Ga₂O₃ was determined to be 10.3 ± 0.2 W/(mK), 19.9 ± 0.2 W/(mK), and 12.6 ± 0.2 W/(mK) along [100], [010], and [001], respectively, aligning with previous experimental measurements. For the first time, we predict the LTC of κ -Ga₂O₃ along [100], [010], and [001] to be 4.5 W/(mK), 3.9 W/(mK), and 4.0 ± 0.1 W/(mK), respectively, showing a nearly isotropic thermal transport property. The reduced LTC of κ -Ga₂O₃ versus β -Ga₂O₃ stems from its restricted low-frequency phonons up to 5 THz. Furthermore, we find that the β phase exhibits a typical temperature dependence slightly stronger than $\sim T^{-1}$, whereas the κ phase shows a weaker temperature dependence, ranging from $\sim T^{-0.5}$ to $\sim T^{-0.7}$.

I. INTRODUCTION

Ultra-wide bandgap semiconductors, such as Ga₂O₃, diamond, AlN, etc., have also become the focus of attention materials for next-generation electronics and optoelectronics. Owing to a bandgap of about 5 eV, exceptional breakdown electrical field, and cost-effective production, Ga₂O₃ offers considerable promise for ultra-high power devices applications.^{1–3} However, the lattice thermal conductivity (LTC) of Ga₂O₃ is subpar, leading to pronounced heat dissipation issues in certain semiconductor devices.¹ Understanding the phonon thermal transport in Ga₂O₃ is crucial for its practical applications.

The Ga₂O₃ crystal actually exists in five distinct phases: α , β , γ , σ , and ε (sometimes referred to as κ). Of these, the β phase (space group C2/m) is the most stable one, which has been extensively explored for applications in deep-ultraviolet transparent conductive electrodes,⁴ solar blind detectors,^{5,6} high-performance field effect transistors,⁷ Schottky rectifiers⁸ and high temperature gas sensors.¹ In recent years, further efforts have been made to overcome the poor thermal stability and immature synthesis methods of other phases. Hexagonal crystal ε -Ga₂O₃ (space group P63mc) was reported to be the second most stable phase obtained at low temperatures^{9,10}, whereas subsequent studies claimed that the crystal structure of the polycrystalline form at low temperatures has an orthorhombic structure at the nanoscale (5 nm–10 nm), named κ -Ga₂O₃ (space group

Pna21).^{11,12} The strong polarization in κ -Ga₂O₃ is a prominent feature that β -Ga₂O₃ does not possess, which may benefit potential device applications. For example, κ -Ga₂O₃ can form heterojunctions with other semiconductors such as GaN or AlN, and its polarization was utilized to regulate interface transport while effectively alleviating thermal problems.^{13,14} Considering the distinct crystal structures of β and κ -Ga₂O₃, a comparative understanding of the LTC for both phases is essential for their device thermal design, particularly as the κ phase remains unexplored.

Currently, growing large-scale single-crystalline κ -Ga₂O₃ is a challenging endeavor experimentally, and assessing its LTC is anticipated to be even more demanding. From a computational perspective, its LTC can be predicted using atomistic simulation techniques, such as molecular dynamics (MD) simulations and the combination of Boltzmann transport equation (BTE) with the anharmonic lattice dynamics (ALD) method. While atomic interactions can be derived from either empirical potentials or quantum mechanical density functional theory (DFT) calculations, intricate crystals like κ -Ga₂O₃, which possess 40 atoms in their primitive cell, introduce substantial hurdles - accuracy concerns for empirical potentials and computational overhead for DFT. Recently, machine-learned potentials (MLPs)-based large-scale MD simulations have been demonstrated to be a reliable approach to calculate the LTC of complex crystals including amorphous silicon¹⁵, amorphous HfO₂¹⁶, amorphous silica¹⁷, metal-organic frameworks¹⁸, and violet phosphorene¹⁹, which can account for phonon anharmonicity to arbitrary order. Several MLPs for Ga₂O₃ have been developed, addressing both the perfect bulk system^{20,21} and more intricate, disordered

^{a)}Electronic mail: hityingph@163.com

^{b)}Electronic mail: huarui.sun@hit.edu.cn

structures^{22,23}.

In this work, we apply the neuroevolution potential (NEP) framework^{24–26} to develop two MLPs on demand for Ga_2O_3 against quantum-mechanical DFT calculations, one for β phase and one for κ phase. We choose the NEP approach here, because this method has been demonstrated to be highly efficient²⁶. We apply the developed NEPs to perform extensive homogeneous non-equilibrium molecular dynamics (HNEMD) simulations to investigate the LTC of the two phases of Ga_2O_3 . Our results show that the LTC of the κ phase is much lower than that of the β phase, and exhibits low anisotropy and weak temperature dependence.

II. METHODS

A. Structural model and DFT calculations

All DFT calculations were performed using projected augmented wave method²⁷ with Perdew-Burke-Ernzerhof functional of generalized gradient approximation²⁸ implemented in the VASP package^{29,30}. The kinetic energy cutoff was set to 520 eV, and the convergence value for the total energy was 1×10^{-6} eV. The stopping criteria for structural optimizations were that the maximum residual Hellmann-Feynman force on atoms was less than 1×10^{-3} eV/Å. A $10 \times 10 \times 6$ and $10 \times 6 \times 6$ Γ -centered k-point grid was employed for the primitive cell of β - Ga_2O_3 and κ - Ga_2O_3 respectively. Additionally, to validate the accuracy of the MLP, the phonon dispersions of β - Ga_2O_3 and κ - Ga_2O_3 were further calculated on $2 \times 2 \times 2$ and $2 \times 1 \times 1$ supercells, respectively, using the density functional perturbation theory together with the PHONOPY package³¹.

Meanwhile, according to widely used conventions, we have optimized the corresponding conventional unit cell as the initial cell for the MD simulation. The κ - Ga_2O_3 lattice structure remains unchanged, but the number of atoms in the conventional unit cell of β - Ga_2O_3 is higher than that in the primitive cell. The calculated lattice constants of β - Ga_2O_3 are $a = 12.468$ Å, $b = 3.087$ Å and $c = 5.716$ Å, while these values for κ - Ga_2O_3 are $a = 5.074$ Å, $b = 8.703$ Å and $c = 9.309$ Å, which are close to reported values^{12,32}. As shown in Figure 1, the conventional unit cell of β - Ga_2O_3 has 20 atoms, while κ - Ga_2O_3 has a relatively large number of 40 atoms. In the calculations of the reference datasets for NEP training, the $2 \times 2 \times 2$ and $2 \times 1 \times 1$ supercells were used for β - Ga_2O_3 and κ - Ga_2O_3 , respectively, with $1 \times 4 \times 2$ and $3 \times 3 \times 3$ k-point grids.

B. The NEP model training

We used the identical method to construct the reference data sets for the β and κ phases of Ga_2O_3 . The reference structures were obtained by *ab initio* molecu-

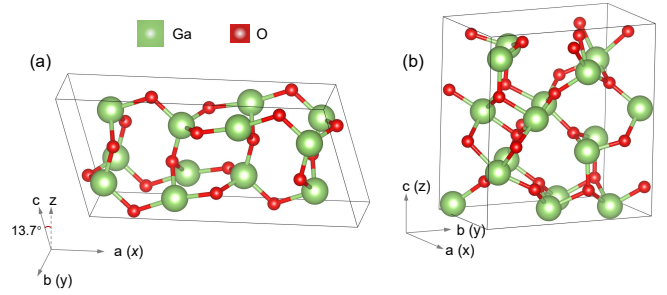


FIG. 1. Crystal structure of the conventional unit cell of (a) β - Ga_2O_3 and (b) κ - Ga_2O_3 .

lar dynamics (AIMD) simulations and random perturbations. For each phase, the AIMD simulations were run under an isothermal ensemble with temperature increasing linearly from 10 K to 1000 K for 10,000 steps and a time step of 1 fs. We uniformly extracted 1,000 structures from AIMD simulations for each case. For random perturbations, 200 structures were generated with random cell deformations ranging from -4% to 4% and atomic displacements less than 0.1 Å, all based on optimized structures. For both phases, our total data set has 1,200 structures including energy, atomic forces, and virials obtained from DFT calculations as outlined in section II A. We randomly divided the total data set into a training set of 1,000 structures and a test set of 200 structures.

After obtaining the training set and test set, we applied the third generation of the NEP framework²⁶ implemented in GPUMD (version 3.5) to train the MLP for β and κ phases of Ga_2O_3 , which were denoted as NEP- β and NEP- κ , respectively. NEP used a feedforward neural network (NN) to represent the site energy with atomic cluster expansion (ACE)³³-like descriptor components including radial and angular terms. The parameters of NEP models were optimized using the separable natural evolution strategy (SNES)³⁴, with the loss function defined as a weighted sum over the root mean square error (RMSE) values of energy, atomic force and virial.

We used the same hyperparameters for these two NEP models. After extensive testing, the selected hyperparameters were determined as follows: the radial and angular cutoffs are $r_c^R = 8$ Å and $r_c^A = 4$ Å, respectively. The number of radial and angular descriptor components are $n_{\max}^R + 1 = 9$ and $n_{\max}^A + 1 = 9$, respectively. For angular parameters, we have $l_{\max}^{3b} = 4$ for three-body and $l_{\max}^{4b} = 2$ for four-body terms, respectively. The number of neurons in the hidden layer of the NN is 50. The size of the population is $N_{\text{pop}} = 50$ and the number of generations is $N_{\text{gen}} = 5 \times 10^5$. The weights of energy, force, and virial RMSEs in the loss function were set to 1.0, 1.0, and 0.1, respectively.

C. Thermal conductivity calculations

We performed MD simulation using the GPUMD package (version 3.5)^{26,35} to calculate the LTCs for the two phases of Ga₂O₃. Based on the HNEMD method, the LTC can be calculated from the relation^{36,37}

$$\frac{\langle J^\mu(t) \rangle_{\text{ne}}}{TV} = \sum_{\nu} \kappa^{\mu\nu} F_e^\nu, \quad (1)$$

where $\kappa^{\mu\nu}$ is the thermal conductivity tensor, T is the system temperature and V is the system volume. The non-equilibrium heat current $\langle J \rangle_{\text{ne}}$ is induced by the external driving force F_i^{ext} related to a driving-force parameter F_e with the dimension of inverse length³⁸

$$F_i^{\text{ext}} = F_e \cdot \mathbf{W}_i. \quad (2)$$

Here, \mathbf{W}_i is the virial tensor of atom i . The magnitude F_e of the driving-force parameter we used for both phases at different temperatures are small enough to keep the system within the linear-response regime.

All MD simulations were conducted at the target temperature using the Nose-Hoover chain method³⁹ with a time step of 1.0 fs. Initially, the simulation was run for 0.1 ns in the isothermal-isobaric ensemble, and subsequently in the isothermal ensemble for 1.0 ns to achieve equilibrium. Afterwards, HNEMD simulations were performed in the isothermal ensemble for 10.0 ns to calculate the running LTCs. We employed $4 \times 16 \times 8$ and $9 \times 5 \times 5$ supercells for β -Ga₂O₃ and κ -Ga₂O₃, respectively, containing 10240 and 9000 atoms. The simulation sizes were validated to be sufficiently large to eliminate finite-size effects. For each case, the predicted LTC was calculated as the average of five independent simulations, and the corresponding standard error was also estimated.

III. RESULTS AND DISCUSSION

A. Validation of the NEP models

Figure 2(a)-(c) show a comparison between the predicted energy, force, and virial values obtained from the NEP models and the corresponding DFT reference values for both the training and test sets of the two phases. In all scenarios, the RMSEs for energy, force, and virial are below 0.5 meV/atom, 40 meV/Å, and 5 meV/atom, respectively. These results demonstrate a very high accuracy of our NEP models. In addition to their high accuracy, our NEPs are remarkably efficient. For a system comprising 10,000 atoms, our NEPs can attain a computational speed of approximately 1.5×10^6 atom-step per second in the GPUMD package using a single GeForce RTX 3090 GPU card. This efficiency enabled us to perform extensive simulations to characterize the LTCs of the Ga₂O₃ crystals.

TABLE I. The predicted LTC tensor (W/(mK)) of (a) β -Ga₂O₃ and (b) κ -Ga₂O₃ from HNEMD simulations at 300 K.

LTC components	β -Ga ₂ O ₃	κ -Ga ₂ O ₃
κ_{xx}	10.3 (0.2)	4.5 (0.0)
κ_{yy}	19.9 (0.2)	3.9 (0.0)
κ_{zz}	12.5 (0.2)	4.0 (0.1)
κ_{xy}	0.2 (0.2)	0.0 (0.1)
κ_{xz}	0.4 (0.2)	0.0 (0.1)
κ_{yz}	0.0 (0.1)	0.0 (0.1)

B. Phonon dispersions

To assess the reliability of our NEP models in capturing the phonon transport properties of β -Ga₂O₃ and κ -Ga₂O₃, we compare the calculated phonon dispersions using both NEP and DFT methods, as shown in Figure 3. It can be seen that for both phases, the acoustic branches predicted by NEP and DFT are very close, while the optical branches of β phase show deviations, especially at high frequencies. Because the theoretical calculation finds that the high-frequency optical branches (>10 THz) contribute minimally to LTC,⁴⁰ which is confirmed by subsequent calculations of the spectrally decomposed LTC in this work. Thus, we believe that the NEP models can reliably predict the LTC of the two phases of Ga₂O₃.

C. Thermal conductivity

After confirming the accuracy of the NEP models, we apply them to calculate LTCs using the HNEMD method. Figure 4 presents the LTCs for both β - and κ -Ga₂O₃ using the HNEMD method at 300 K. Notably, Figure 1(a) reveals that β -Ga₂O₃ possesses a monoclinic crystal structure, suggesting the potential for non-zero values in the off-diagonal elements in the LTC tensor. Fortunately, the HNEMD approach (see Equation 1) allows us to fully determine the LTC tensor as listed in Table I, by applying the external driving force along three orthogonal axes sequentially. As anticipated, the β phase exhibits minor couplings between the x and z directions. In contrast, the off-diagonal elements of the LTC tensor for the κ phase are zero, attributed to its orthorhombic crystal structure.

Based on the polar coordinates as shown in Figure 5(a), we can determine the LTC along any crystal direction:⁴¹

$$\kappa(\theta, \phi) = \boldsymbol{\alpha} \begin{pmatrix} \kappa_{xx} & \kappa_{xy} & \kappa_{xz} \\ \kappa_{xy} & \kappa_{yy} & \kappa_{yz} \\ \kappa_{xz} & \kappa_{yz} & \kappa_{zz} \end{pmatrix} \boldsymbol{\alpha}^T, \quad (3)$$

with

$$\boldsymbol{\alpha} = (\sin \phi \cos \theta, \sin \phi \sin \theta, \cos \phi). \quad (4)$$

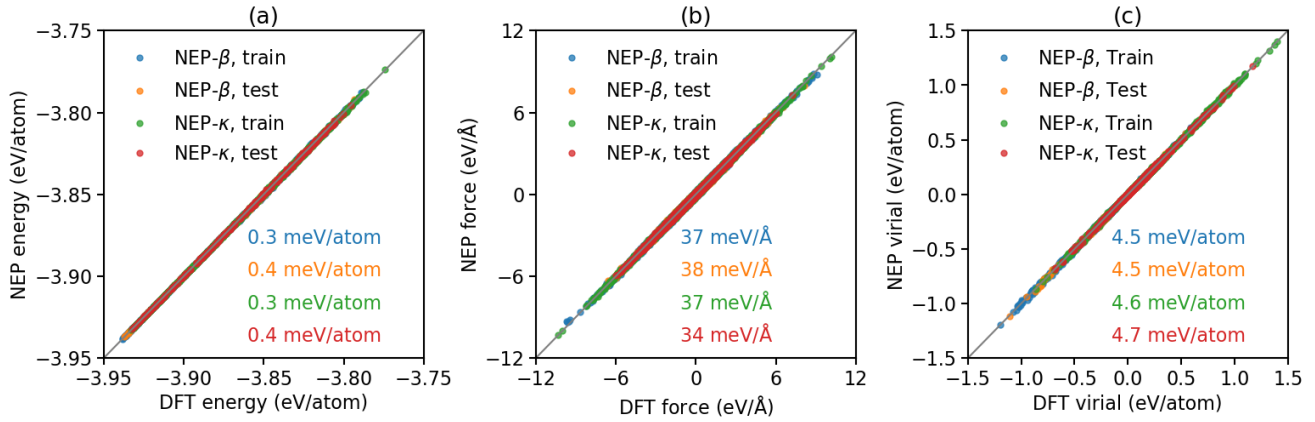


FIG. 2. The NEP predictions of energy, force, and virial for train and test sets against the DFT reference values.

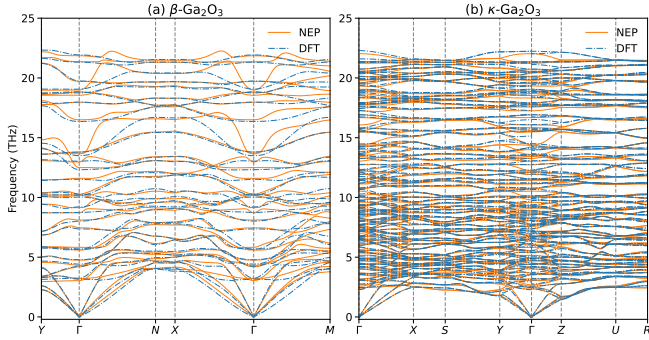


FIG. 3. The phonon dispersions of (a) β -Ga₂O₃ and (b) κ -Ga₂O₃ predicted by NEP and DFT.

Figure 5(b) and (c) show the 3D distribution of LTC for the β and κ phases, respectively. The corresponding 2D projection in the [001], [010], and [100]-planes are presented in Figure 5(d)-(f), respectively.

For the β phase, the LTC is highest along the [010] direction with 19.9 ± 0.2 W/(mK), followed by [001] with 12.6 ± 0.2 W/(mK) (see the blue dotted line in Figure 5(e)), and [100] at 10.3 ± 0.2 W/(mK). As shown in Table II, our HNEMD results are consistent with previous experimental results^{41,42} using time-domain thermoreflectance and theoretical predictions based on the BTE-ALD method^{20,40,43,44} or the equilibrium molecular dynamics (EMD) method²¹. This further demonstrates the reliability of our HNEMD approach based on machine-learned NEP in characterizing the LTC of Ga₂O₃ crystals.

To our knowledge, the LTC of κ -Ga₂O₃ has not been investigated before. Here, we predict the LTC for κ -Ga₂O₃ to be 4.5 W/(mK), 3.9 W/(mK), and 4.0 ± 0.1 W/(mK) along the [100], [010], and [001] directions, respectively. These values are about one-fifth to half of those of β -Ga₂O₃. While the β phase displays a significant LTC anisotropy with an anisotropy index of 1.94

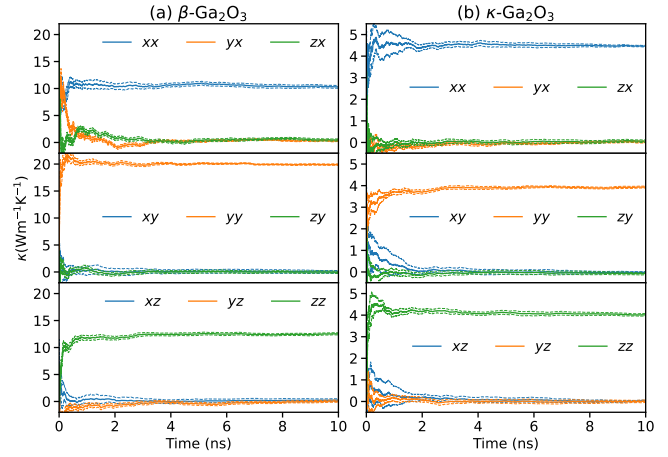


FIG. 4. Running LTC tensors from HNEMD simulations at 300K for: (a) β - and (b) κ -Ga₂O₃. Driving forces for top, middle, and bottom are along the x , y , and z directions, respectively.

(the maximum-to-minimum ratio of the LTC, see spatial distribution in Figure 5(b)), the κ phase exhibits a nearly isotropic LTC pattern with an anisotropy index of 1.15. (see Figure 5(c)).

To elucidate the disparities in the LTC observed between the two phases, we decomposed the LTC as a function of phonon frequency:³⁷

$$\kappa^{\mu\nu}(\omega) = \frac{2}{VTF_e^\nu} \int_{-\infty}^{\infty} dt e^{i\omega t} K^{\mu\nu}(t). \quad (5)$$

Here $K(t) = \sum_i \langle \mathbf{W}_i(0) \cdot \mathbf{v}_i(t) \rangle$ is the virial-velocity correlation function³⁸, in which \mathbf{W}_i and \mathbf{v}_i are the virial tensor and the velocity of atom i , respectively.

Figure 6 presents the spectrally decomposed LTC of β -Ga₂O₃ and κ -Ga₂O₃ calculated from Equation 5. Taken as a whole, only phonon modes with frequencies in the 0–10 THz range are really involved in thermal transport.

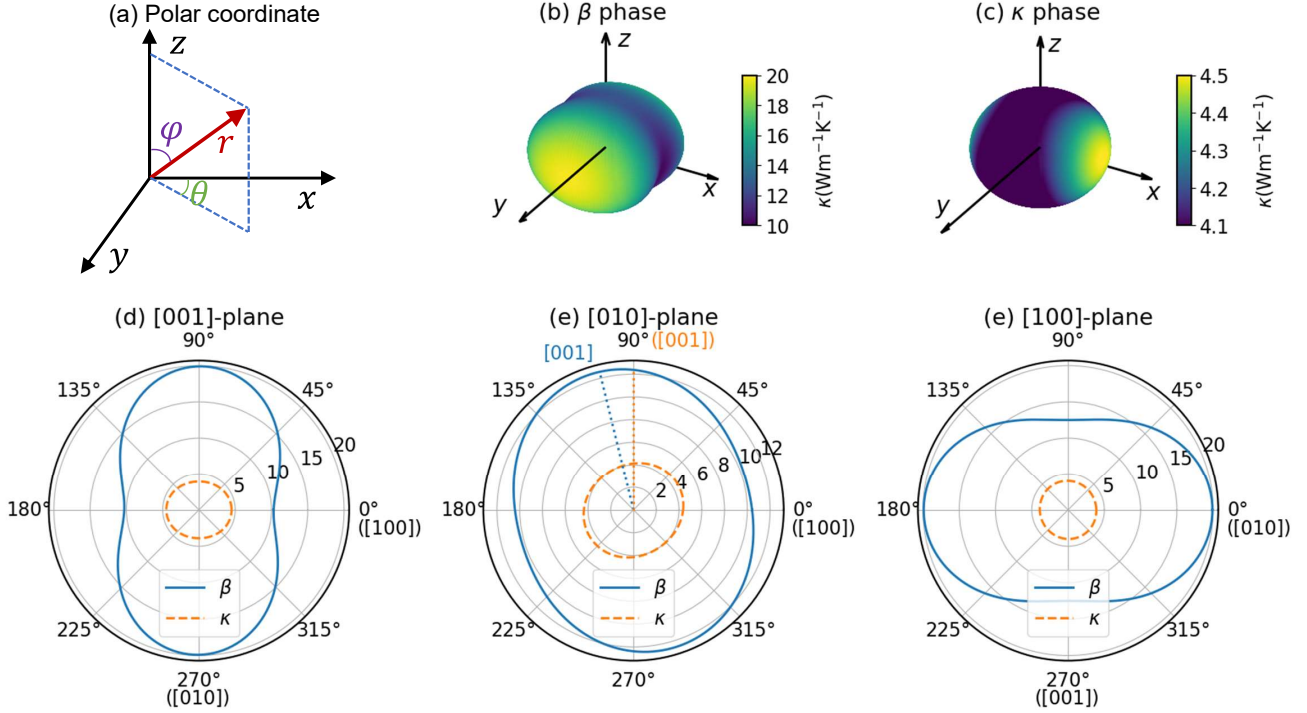


FIG. 5. (a) The polar coordination used for the transformation of the LTC tensor. (b) and (c) The 3D distributions of the LTC for β -Ga₂O₃ and κ -Ga₂O₃. (d), (e), and (f) The corresponding 2D projections onto the [100], [010], and [001]-planes, respectively. All LTCs are in units of W/(mK).

TABLE II. The LTC (W/(mK)) of β -Ga₂O₃ at 300 K predicted by our HNEMD simulations and previously reported values. The values in parentheses denote the standard errors.

Method	[100]	[010]	[001]
Current HNEMD	10.3 (0.2)	19.9 (0.2)	12.6 (0.2)
Experiment ⁴¹	9.5 (1.8)	22.5 (2.5)	13.3 (1.8)
Experiment ⁴²	10.9 (1.0)	27.0 (2.0)	15.0
EMD ²¹	10.7	20.8	12.6
BTE-ALD ²⁰	13.9	24.8	19.8
BTE-ALD ⁴³	16.1	21.5	21.2
BTE-ALD ⁴⁰	12.7	20.0	17.8
BTE-ALD ⁴⁴	10.02	23.74	12

It also can be found that, although in both phases the low-frequency acoustic phonons contribute significantly to the LTC, the β phase has a much broader distribution of phonon frequencies contributing to its LTC than the κ phase. This is also related to the the phonon dispersions as shown in Figure 3. The branches of the κ phase with a phonon frequency in the range of 5 THz to 10 THz are much flatter than those of the β phase, leading to much lower phonon group velocities. Moreover, in the κ phase, we observe significant overlaps between multiple bands for phonon frequencies greater than 3 THz, indicating the

presence of multiple scattering channels, a phenomenon previously observed in Violet phosphorene¹⁹.

Furthermore, Figure 7 shows the temperature-dependent LTC for β - and κ -Ga₂O₃. In the temperature range of 200 K to 600 K, the LTCs of both phases decrease with increasing temperature. The LTC of the β phase exhibits a temperature dependence slightly stronger than $\sim T^{-1}$, as typical for systems dominated by three-phonon scattering processes⁴⁵. However, the LTC of κ -Ga₂O₃ shows a clearly weaker temperature dependence, which is $\sim T^{-0.5}$ along the [100] direction and $\sim T^{-0.7}$ along the the [010] and [001] directions, suggesting a significant impact of higher-order anharmonic phonon scatterings attributable to its complex crystal structures⁴⁶.

IV. CONCLUSIONS

In summary, we have developed machine-learned NEP models trained against quantum-mechanical DFT data for the β and κ phases of Ga₂O₃, which have been demonstrated to be accurate and efficient in predicting energy, atomic forces, virial, and phonon dispersions in both phases. Based on large-scale HNEMD simulations, we reached a consistent prediction with previous experimental measurements for the β phase, and predicted the LTC of the κ phase for the first time. We found that the κ phase has a much lower LTC than the β phase, due to

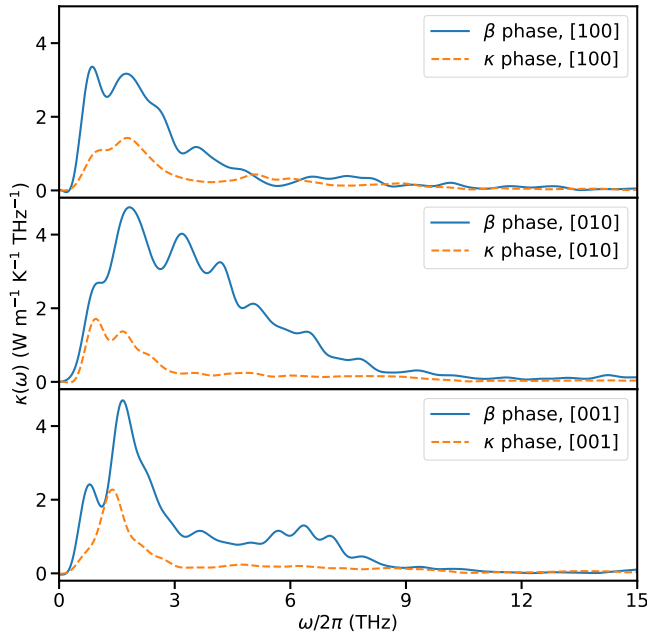


FIG. 6. The spectrally decomposed LTC of (a) β -Ga₂O₃ and (b) κ -Ga₂O₃ as a function of phonon frequency.

its phonon frequency contributions being limited to below 5 THz compared to the 0 THz to 10 THz range of the β phase. Furthermore, the κ phase exhibits an almost isotropic spatial distribution with an anisotropy index of 1.15 at 300 K, in contrast to the pronounced anisotropy index of 1.94 for the β phase. We also examined the temperature dependence of the LTC in the two phases, and found that the LTC of the β phase follows a temperature dependence slightly stronger than $\sim T^{-1}$, whereas the κ phase shows a weaker temperature dependence from $\sim T^{-0.5}$ to $\sim T^{-0.7}$, indicating a significant effect of high-order anharmonicity distinct as in low-LTC materials. Our work demonstrates that the machine-learned NEP-driven HNEMD simulations can reliably and effectively characterize phonon thermal transport properties for complex crystals such as κ -Ga₂O₃, and thus we expect that this approach can be used to explore the LTCs of other phases of Ga₂O₃ as well.

ACKNOWLEDGMENTS

This work was supported by the Key-Area Research and Development Program of Guangdong Province (Grant No.2020B010169002), the Guangdong Special Support Program (Grant No.2021TQ06C953), and the Science and Technology Planning Project of Shenzhen Municipality (Grant No. JCYJ20190806142614541).

Conflict of Interest

The authors have no conflicts to disclose.

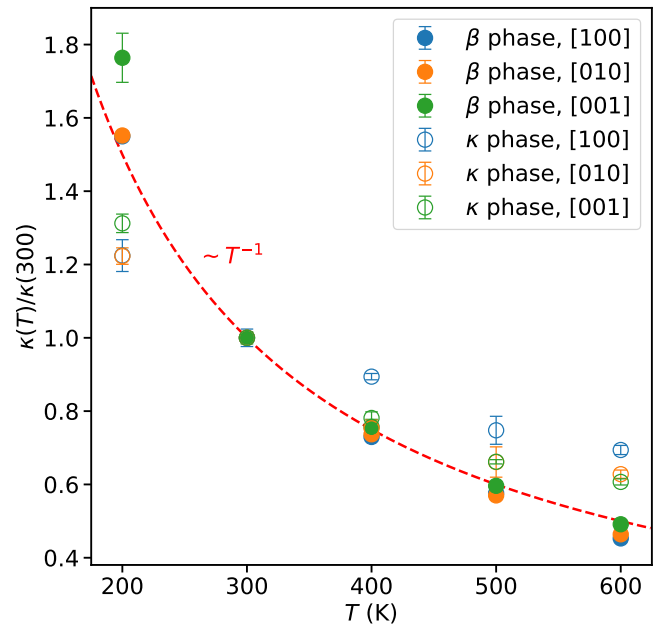


FIG. 7. LTC of β and κ phases of Ga₂O₃ as a function of temperature T along three directions. All the LTCs are normalized by their values at 300 K, respectively.

Data availability Complete input and output files for the NEP training of β -Ga₂O₃ and κ -Ga₂O₃ crystals are freely available at <https://gitlab.com/brucefan1983/nep-data>. The source code and documentation for GPUMD are available at <https://github.com/brucefan1983/GPUMD> and <https://gpumd.org>, respectively.

REFERENCES

- ¹S. Pearton, J. Yang, P. H. Cary, F. Ren, J. Kim, M. J. Tadjer, and M. A. Mastro, “A review of Ga₂O₃ materials, processing, and devices,” *Applied Physics Reviews* **5** (2018), 10.1063/1.5006941.
- ²J. Zhang, P. Dong, K. Dang, Y. Zhang, Q. Yan, H. Xiang, J. Su, Z. Liu, M. Si, J. Gao, *et al.*, “Ultra-wide bandgap semiconductor Ga₂O₃ power diodes,” *Nature Communications* **13**, 3900 (2022).
- ³N. Ueda, H. Hosono, R. Waseda, and H. Kawazoe, “Anisotropy of electrical and optical properties in β -Ga₂O₃ single crystals,” *Applied physics letters* **71**, 933–935 (1997).
- ⁴M. Orita, H. Ohta, M. Hirano, and H. Hosono, “Deep-ultraviolet transparent conductive β -Ga₂O₃ thin films,” *Applied Physics Letters* **77**, 4166–4168 (2000).
- ⁵P. Feng, J. Y. Zhang, Q. H. Li, and T. H. Wang, “Individual β -Ga₂O₃ nanowires as solar-blind photodetectors,” *Applied Physics Letters* **88**, 153107 (2006).
- ⁶X. Zhou, M. Li, J. Zhang, L. Shang, K. Jiang, Y. Li,

- L. Zhu, J. Chu, and Z. Hu, “Flexible solar-blind photodetectors based on β -Ga₂O₃ films transferred by a stamp-based printing technique,” *IEEE Electron Device Letters* **43**, 1921–1924 (2022).
- ⁷W. S. Hwang, A. Verma, H. Peelaers, V. Protasenko, S. Rouvimov, A. Seabaugh, W. Haensch, C. V. de Walle, Z. Galazka, M. Albrecht, *et al.*, “High-voltage field effect transistors with wide-bandgap β -Ga₂O₃ nanomembranes,” *Applied Physics Letters* **104** (2014), 10.1063/1.4879800.
- ⁸S. J. Pearton, F. Ren, M. Tadjer, and J. Kim, “Perspective: Ga₂O₃ for ultra-high power rectifiers and MOSFETS,” *Journal of Applied Physics* **124**, 220901 (2018).
- ⁹H. Y. Playford, A. C. Hannon, E. R. Barney, and R. I. Walton, “Structures of uncharacterised polymorphs of gallium oxide from total neutron diffraction,” *Chemistry—A European Journal* **19**, 2803–2813 (2013).
- ¹⁰Y. Zhuo, Z. Chen, W. Tu, X. Ma, Y. Pei, and G. Wang, “ β -Ga₂O₃ versus ϵ -Ga₂O₃: Control of the crystal phase composition of gallium oxide thin film prepared by metal-organic chemical vapor deposition,” *Applied Surface Science* **420**, 802–807 (2017).
- ¹¹I. Cora, F. Mezzadri, F. Boschi, M. Bosi, M. Čaplovičová, G. Calestani, I. Dódony, B. Pécz, and R. Fornari, “The real structure of ϵ -Ga₂O₃ and its relation to κ -phase,” *CrystEngComm* **19**, 1509–1516 (2017).
- ¹²B. M. Janzen, P. Mazzolini, R. Gillen, V. F. Peltason, L. P. Grote, J. Maultzsch, R. Fornari, O. Bierwagen, and M. R. Wagner, “Comprehensive raman study of orthorhombic κ/ϵ -Ga₂O₃ and the impact of rotational domains,” *Journal of Materials Chemistry C* **9**, 14175–14189 (2021).
- ¹³Y. Chen, H. Ning, Y. Kuang, X.-X. Yu, H.-H. Gong, X. Chen, F.-F. Ren, S. Gu, R. Zhang, Y. Zheng, *et al.*, “Band alignment and polarization engineering in κ -Ga₂O₃/GaN ferroelectric heterojunction,” *Science China Physics, Mechanics & Astronomy* **65**, 277311 (2022).
- ¹⁴S. Krishna, Y. Lu, C.-H. Liao, V. Khandelwal, and X. Li, “Band alignment of orthorhombic Ga₂O₃ with gan and aln semiconductors,” *Applied Surface Science* **599**, 153901 (2022).
- ¹⁵Y. Wang, Z. Fan, P. Qian, M. A. Caro, and T. Ala-Nissila, “Quantum-corrected thickness-dependent thermal conductivity in amorphous silicon predicted by machine learning molecular dynamics simulations,” *Physical Review B* **107**, 054303 (2023).
- ¹⁶H. Zhang, X. Gu, Z. Fan, and H. Bao, “Vibrational anharmonicity results in decreased thermal conductivity of amorphous HfO₂ at high temperature,” *Phys. Rev. B* **108**, 045422 (2023).
- ¹⁷T. Liang, P. Ying, K. Xu, Z. Ye, C. Ling, Z. Fan, and J. Xu, “Mechanisms of temperature-dependent thermal transport in amorphous silica from machine-learning molecular dynamics,” (2023), arXiv:2310.09062 [cond-mat.mtrl-sci].
- ¹⁸P. Ying, T. Liang, K. Xu, J. Zhang, J. Xu, Z. Zhong, and Z. Fan, “Sub-Micrometer Phonon Mean Free Paths in Metal–Organic Frameworks Revealed by Machine Learning Molecular Dynamics Simulations,” *ACS Applied Materials & Interfaces* **15**, 36412–36422 (2023).
- ¹⁹P. Ying, T. Liang, K. Xu, J. Xu, Z. Fan, T. Ala-Nissila, and Z. Zhong, “Variable thermal transport in black, blue, and violet phosphorene from extensive atomistic simulations with a neuroevolution potential,” *International Journal of Heat and Mass Transfer* **202**, 123681 (2023).
- ²⁰Y. Liu, J. Yang, G. Xin, L. Liu, G. Csányi, and B. Cao, “Machine learning interatomic potential developed for molecular simulations on thermal properties of β -Ga₂O₃,” *The Journal of Chemical Physics* **153**, 144501 (2020).
- ²¹R. Li, Z. Liu, A. Rohskopf, K. Gordiz, A. Henry, E. Lee, and T. Luo, “A deep neural network interatomic potential for studying thermal conductivity of β -Ga₂O₃,” *Applied Physics Letters* **117**, 152102 (2020).
- ²²J. Zhao, J. Byggmästar, H. He, K. Nordlund, F. Djurabekova, and M. Hua, “Complex Ga₂O₃ polymorphs explored by accurate and general-purpose machine-learning interatomic potentials,” *npj Computational Materials* **9**, 159 (2023).
- ²³Y. Liu, H. Liang, L. Yang, G. Yang, H. Yang, S. Song, Z. Mei, G. Csányi, and B. Cao, “Unraveling thermal transport correlated with atomistic structures in amorphous gallium oxide via machine learning combined with experiments,” *Advanced Materials* **35**, 2210873 (2023).
- ²⁴Z. Fan, Z. Zeng, C. Zhang, Y. Wang, K. Song, H. Dong, Y. Chen, and T. Ala-Nissila, “Neuroevolution machine learning potentials: Combining high accuracy and low cost in atomistic simulations and application to heat transport,” *Phys. Rev. B* **104**, 104309 (2021).
- ²⁵Z. Fan, “Improving the Accuracy of the Neuroevolution Machine Learning Potential for Multi-Component Systems,” *Journal of Physics: Condensed Matter* **34**, 125902 (2022).
- ²⁶Z. Fan, Y. Wang, P. Ying, K. Song, J. Wang, Y. Wang, Z. Zeng, K. Xu, E. Lindgren, J. M. Rahm, A. J. Gabourie, J. Liu, H. Dong, J. Wu, Y. Chen, Z. Zhong, J. Sun, P. Erhart, Y. Su, and T. Ala-Nissila, “GPUMD: A package for constructing accurate machine-learned potentials and performing highly efficient atomistic simulations,” *The Journal of Chemical Physics* **157**, 114801 (2022).
- ²⁷P. E. Blöchl, “Projector augmented-wave method,” *Physical review B* **50**, 17953 (1994).
- ²⁸J. P. Perdew, K. Burke, and M. Ernzerhof, “Generalized gradient approximation made simple,” *Physical review letters* **77**, 3865 (1996).
- ²⁹G. Kresse and J. Furthmüller, “Efficient Iterative Schemes for Ab Initio Total-Energy Calculations Using a Plane-Wave Basis Set,” *Physical Review B* **54**, 11169 (1996).

- ³⁰G. Kresse and D. Joubert, “From ultrasoft pseudopotentials to the projector augmented-wave method,” *Physical Review B* **59**, 1758 (1999).
- ³¹A. Togo and I. Tanaka, “First principles phonon calculations in materials science,” *Scripta Materialia* **108**, 1–5 (2015).
- ³²J. Åhman, G. Svensson, and J. Albertsson, “A reinvestigation of β -gallium oxide,” *Acta Crystallographica Section C: Crystal Structure Communications* **52**, 1336–1338 (1996).
- ³³R. Drautz, “Atomic cluster expansion for accurate and transferable interatomic potentials,” *Physical Review B* **99**, 014104 (2019).
- ³⁴T. Schaul, T. Glasmachers, and J. Schmidhuber, “High Dimensions and Heavy Tails for Natural Evolution Strategies,” in *Proceedings of the 13th Annual Conference on Genetic and Evolutionary Computation, GECCO '11* (Association for Computing Machinery, New York, NY, USA, 2011) pp. 845–852.
- ³⁵Z. Fan, W. Chen, V. Vierimaa, and A. Harju, “Efficient Molecular Dynamics Simulations with Many-Body Potentials on Graphics Processing Units,” *Computer Physics Communications* **218**, 10–16 (2017).
- ³⁶D. J. Evans, “Homogeneous NEMD algorithm for thermal conductivity—Application of non-canonical linear response theory,” *Physics Letters A* **91**, 457–460 (1982).
- ³⁷Z. Fan, H. Dong, A. Harju, and T. Ala-Nissila, “Homogeneous Nonequilibrium Molecular Dynamics Method for Heat Transport and Spectral Decomposition with Many-Body Potentials,” *Physical Review B* **99**, 064308 (2019).
- ³⁸A. J. Gabourie, Z. Fan, T. Ala-Nissila, and E. Pop, “Spectral decomposition of thermal conductivity: Comparing velocity decomposition methods in homogeneous molecular dynamics simulations,” *Physical Review B* **103**, 205421 (2021).
- ³⁹M. E. Tuckerman, *Statistical mechanics: theory and molecular simulation* (Oxford university press, 2023).
- ⁴⁰Z. Yan and S. Kumar, “Phonon mode contributions to thermal conductivity of pristine and defective β -Ga₂O₃,” *Phys. Chem. Chem. Phys.* **20**, 29236–29242 (2018).
- ⁴¹P. Jiang, X. Qian, X. Li, and R. Yang, “Three-dimensional anisotropic thermal conductivity tensor of single crystalline β -Ga₂O₃,” *Applied Physics Letters* **113**, 232105 (2018).
- ⁴²Z. Guo, A. Verma, X. Wu, F. Sun, A. Hickman, T. Masui, A. Kuramata, M. Higashiwaki, D. Jena, and T. Luo, “Anisotropic thermal conductivity in single crystal β -Ga₂O₃,” *Applied Physics Letters* **106**, 111909 (2015).
- ⁴³M. D. Santia, N. Tandon, and J. Albrecht, “Lattice thermal conductivity in β -Ga₂O₃ from first principles,” *Applied Physics Letters* **107** (2015), 10.1063/1.4927742.
- ⁴⁴Y. Chen, L. Peng, Y. Wu, C. Ma, A. Wu, H. Zhang, and Z. Fang, “Anomalous Temperature-Dependent Phonon Anharmonicity and Strain Engineering of Thermal Conductivity in β -Ga₂O₃,” *The Journal of Physical Chemistry C* **127**, 13356–13363 (2023).
- ⁴⁵L. Lindsay, D. A. Broido, and T. L. Reinecke, “Ab initio thermal transport in compound semiconductors,” *Phys. Rev. B* **87**, 165201 (2013).
- ⁴⁶L. Lindsay, A. Katre, A. Cepellotti, and N. Mingo, “Perspective on ab initio phonon thermal transport,” *Journal of Applied Physics* **126**, 050902 (2019).